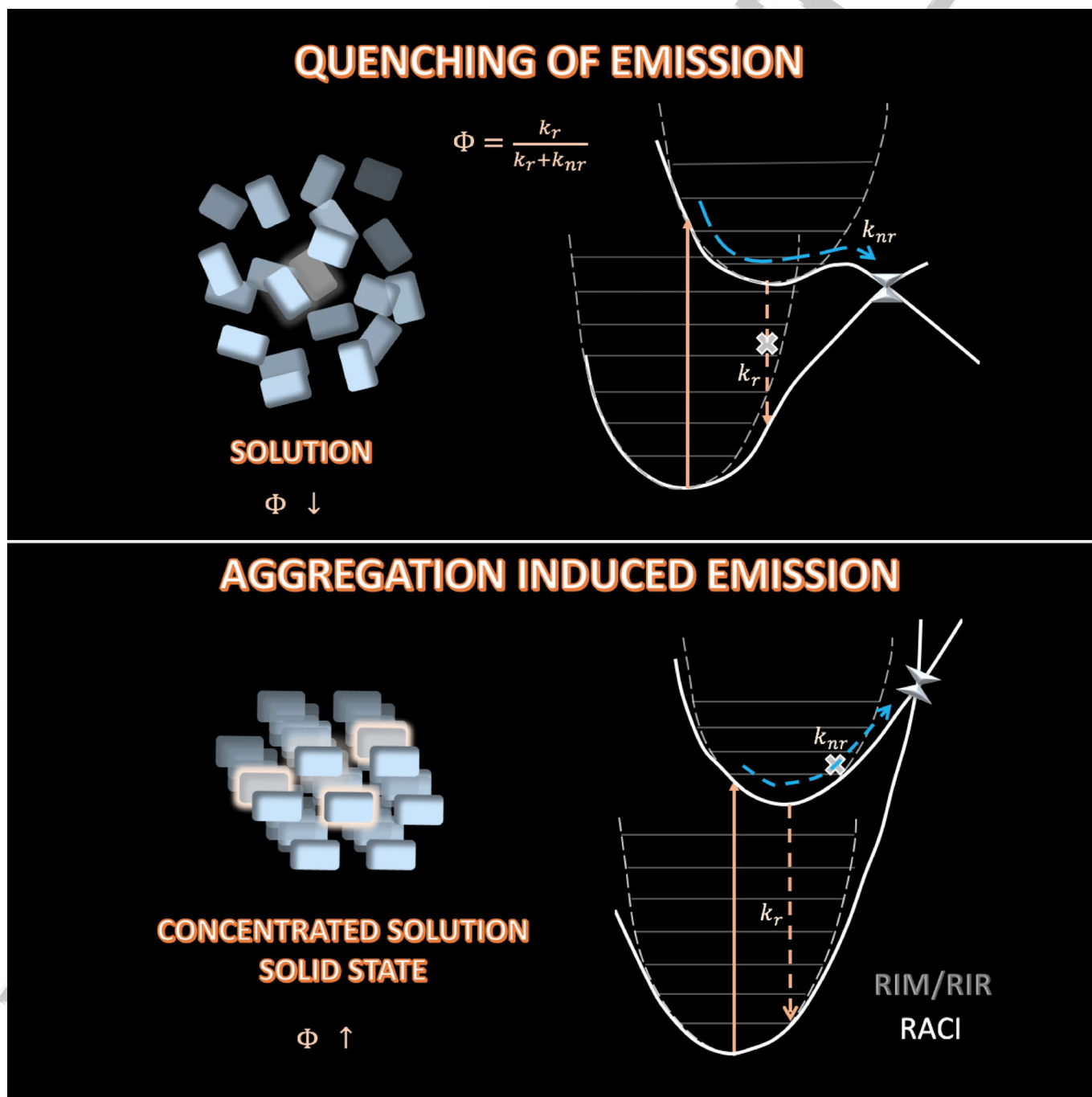


1  
2  
3  
4  
5  
6  
7  
8  
9  
10  
11  
12  
13  
14  
15  
16  
17  
18  
19  
20  
21  
22  
23  
24  
25  
26  
27  
28  
29  
30  
31  
32  
33  
34  
35  
36  
37  
38  
39  
40  
41  
42  
43  
44  
45  
46  
47  
48  
49  
50  
51  
52  
53  
54  
55  
56  
57

SPECIAL  
ISSUE

# Exploring Potential Energy Surfaces for Aggregation-Induced Emission—From Solution to Crystal

Rachel Crespo-Otero,<sup>\*,[b]</sup> Quansong Li,<sup>[c]</sup> and Lluís Blancafort<sup>\*,[a]</sup>



**Abstract:** Aggregation-induced emission (AIE) is a phenomenon where non-luminescent compounds in solution become strongly luminescent in aggregate and solid phase. It provides a fertile ground for luminescent applications that has rapidly developed in the last 15 years. In this review, we focus on the contributions of theory and computations to understanding the molecular mechanism behind it. Starting from initial models, such as restriction of intramolecular rotations (RIR), and the calculation of non-radiative rates with Fermi's golden rule (FGR), we center on studies of the global

excited-state potential energy surfaces that have provided the basis for the restricted access to a conical intersection (RACI) model. In this model, which has been shown to apply for a diverse group of AIEgens, the lack of fluorescence in solution comes from radiationless decay at a CI in solution that is hindered in the aggregate state. We also highlight how intermolecular interactions modulate the photophysics in the aggregate phase, in terms of fluorescence quantum yield and emission color.

## 1. Introduction

Highly emissive materials based on organic  $\pi$ -conjugated molecules find applications in display technologies, optical communication, data storage, biological sensing, and solid-state lasing (see Ref. [1] and references therein). Design of new materials with improved properties is an important goal that encounters substantial difficulties. Most applications are implemented in the condensed phase (solution, film, or solid state), but the luminescent properties of the materials are often significantly different from the photophysics of their components at the molecular level. The differences can also be difficult to predict, posing additional difficulties for the design.

One frequent drawback is a significant reduction of the emissive response associated with the formation of aggregates in the condensed phase. Aggregation quenching results from the formation of  $\pi$ - $\pi$  and charge transfer (CT) aggregates promoting deactivation through non-radiative pathways competing with radiative emission.<sup>[2]</sup> The opposite phenomenon, where compounds that are not or only weakly emissive in solution become fluorescent in the aggregate phase, provides a route for the design of luminescent materials. It is usually referred to as aggregation-induced emission (AIE), a term that

was coined in 2001 by Tang et al. to describe the enhancement of emission observed for 1-methyl-1,2,3,4,5-pentaphenylsilole in concentrated solution.<sup>[3-6]</sup> The quest for chromophores exhibiting AIE (AIEgens) has become a very active field of research in the last 15 years.<sup>[4-10]</sup>

In this rapidly expanding field, theory and computations have aimed at identifying the mechanism(s) and molecular features behind AIE to provide design principles for more efficient emitters. The key quantity is the fluorescence yield  $\Phi_f$ , which is related by Equation (1) to the radiative and non-radiative rates,  $k_r$  and  $k_{nr}$ :

$$\Phi_f = \frac{k_r}{k_r + k_{nr}} \quad (1)$$

Radiative processes include fluorescence ( $k_f$ ) and phosphorescence ( $k_{ph}$ ), and non-radiative processes internal conversion (IC) and intersystem crossing (ISC) to  $S_0$  [Eqs. (2) and (3), respectively]:

$$k_r = k_f + k_{ph} \quad (2)$$


$$k_{nr} = k_{IC,S_0} + k_{ISC,S_0} \quad (3)$$


These processes are illustrated with a typical potential energy surface (PES) in Figure 1. Enhanced emission can be due to restriction of non-radiative mechanisms and/or an increase of the radiative emission probability,<sup>[1,11,12]</sup> and theoretical studies have evaluated different mechanisms for each case. As we explain briefly in the next section, one of the most widely used approaches in the field is based on calculation of non-radiative rates by using Fermi's golden rule (FGR). This approach to AIE has been revised recently,<sup>[10,13]</sup> and in this focus review we center on alternative approaches that consider the global potential energy surface, and in particular the role of conical intersections (CIs), discussing also the differences and complementarities between the two approaches. In the final section, we discuss the importance of intermolecular interactions, focusing on the difference between steric and electronic aggregation effects and how they have been considered theoretically.

[a] Prof. L. Blancafort  
Institut de Química Computacional i Catàlisi (IQCC) i Departament de Química  
Facultat de Ciències  
Universitat de Girona  
C/M. A. Capmany 69, 17003 Girona (Spain)  
E-mail: lluis.blancafort@udg.edu

[b] Dr. R. Crespo-Otero  
School of Biological and Chemical Sciences  
Queen Mary University of London  
Mile End Road, London E1 4NS (United Kingdom)  
E-mail: r.crespo-otero@qmul.ac.uk

[c] Prof. Q. Li  
School of Chemistry and Chemical Engineering  
Beijing Institute of Technology  
South Zhongguancun Street 5, 100081 Beijing (China)

 The ORCID identification number(s) for the author(s) of this article can be found under:  
<https://doi.org/10.1002/asia.201801649>.

 This manuscript is part of a special issue on aggregation-induced emission. A link to the Table of Contents of the special issue will appear here when the complete issue is published.

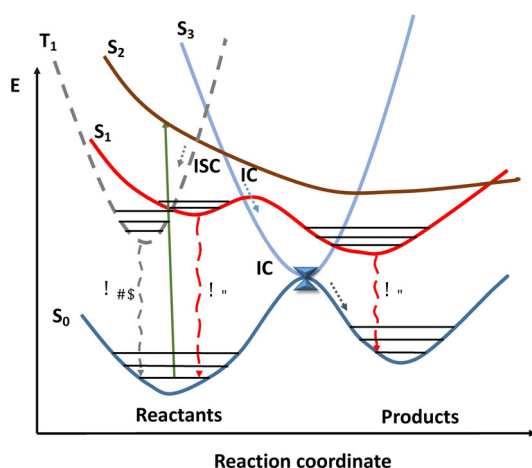


Figure 1. Radiative (r) and non-radiative (nr) processes in a typical PES. Only a few vibrational states are shown for illustrative purposes.

## 2. Intramolecular Restriction Models and FGR-based Calculations

### 2.1. Intramolecular restriction models

The initial explanation of AIE was based on the assumption that non-radiative mechanisms are restricted in the aggregate phase, and the idea that the lack of emission in solution may be due to transfer of the electronic excitation energy to low-frequency intramolecular rotational modes.<sup>[14]</sup> These modes have a high density of vibrational states, which may make them ideal “acceptors” of the excitation. In the aggregate phase, these motions are hindered and the electronic to vibrational energy conversion may not be possible anymore, causing the molecules to emit. This mechanism is termed restriction of intramolecular rotations (RIR) and is consistent with the fact that many molecules showing AIE have a similar structure: a cyclic “core” unit acting as chromophore (e.g., silole, dibenzofulvene, etc.), and a relatively large number of phenyl substituents attached to the core.<sup>[5]</sup> The low-frequency modes responsible for accepting the energy are the rotations of the phenyl substituents. The model was later extended to account for the fact that other low-frequency modes may also be responsible for energy dissipation, leading to the restriction of intramolecular motions (RIM) mechanism.<sup>[15]</sup> The RIR and RIM models have been used successfully for the design of numerous AIE emitters but as we discuss below, they cannot explain, for instance, some results where structurally similar compounds show different luminescent properties.

### 2.2. The FGR-based approach

From the computational side, the RIR and RIM mechanisms have been supported by Fermi golden rule (FGR) calculations under the harmonic approximation.<sup>[10–13,16–27]</sup> Different levels of approximations have been used to evaluate the radiative and non-radiative constants,  $k_r$  and  $k_{nr}$ .<sup>[10–13,16–21,24–27]</sup> The simplest model is based on the displaced harmonic approximation, where the PES of the excited state is obtained as a rigid dis-

placement of the ground state PES.<sup>[22,28]</sup> In AIEgens dominated by the RIM mechanism, the reorganization energies of the modes with larger contributions to the internal conversion rate,  $k_{IC}$ , are hampered in the aggregated state owing to the steric restrictions. In this context, the evaluation of the Huang–Rhys factors,  $S_j$ , and the reorganization energies,  $\lambda_{ij}$ , have become very popular for the semi-quantitative interpretation of AIE.<sup>[10,12,21–23,25,26,29–34]</sup>

The most sophisticated approaches include the consideration of the mixing between the excited and ground state vibrations by using Duschinsky rotation matrices and the path integral framework.<sup>[11,23,35]</sup> These approaches have been implemented in a code called MOMAP.<sup>[11]</sup> Transition dipole moments, non-adiabatic couplings, and spin–orbit couplings are required for the evaluation of  $k_r$  and  $k_{nr}$  constants. The details of the formalism and the complete mathematical developments can be

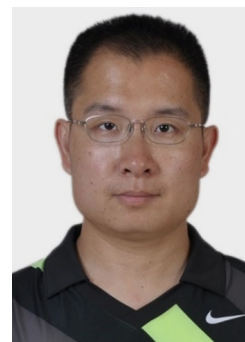
Lluís Blancafort received his degree in chemical engineering at the Institut Químic de Sarrià (Barcelona) in 1991. He obtained his Ph.D. in 1996 from the University of Würzburg, for research on the reactivity of  $\alpha$ -peroxy lactones. From 1997 to 2002, he carried out a postdoctoral research at King's College London, working on the computation of excited-state mechanisms. In 2002, he joined the University of Girona as a Ramón y Cajal fellow and became associate professor in 2007. His main research interests are the theory and computation of excited states and non-adiabatic processes, including excited-state potential energy surfaces and dynamics.



Rachel Crespo Otero did her Ph.D. within a collaborative program between the University of Havana and the Autonomous University of Madrid. From 2010 to 2013, she worked on the development and application of methods to investigate non-adiabatic dynamics in the group of Prof. M. Barbatti at the Max Planck Institute for Coal Research (Mülheim an der Ruhr, Germany). In 2013, she joined the group of Prof. Aron Walsh at the University of Bath in the UK to work on metastable materials and water splitting. Since 2015, she has been a Lecturer in Computational Chemistry at Queen Mary University of London. Her research focuses on the investigation of excited states and non-adiabatic processes at the frontier of molecular and materials sciences.



Quansong Li was born in Shandong province, China (1978). He received his B.Sc. (2001) and Ph.D. (2006) degrees at Beijing Normal University. After his postdoctoral work at City University of Hong Kong (2006–2008) and the University of Girona (2008–2012), he joined Beijing Institute of Technology as an associate professor in 2013 and became a full professor in 2018. His main research interests are in computational photochemistry, including mechanisms of photoinduced processes and design of materials for solar cells.



found in references [11] and [18]. These calculations have reproduced temperature effects<sup>[23,27]</sup> on the non-radiative rates as well as isotope effects<sup>[36]</sup> in the solid phase. A comparison of the reorganization energies with the cross-sections obtained from resonance Raman spectroscopy<sup>[27]</sup> has provided further experimental support for this model, which has been extended to include the effect of exciton coupling.<sup>[24]</sup>

From the point of view of computational cost, FGR rate calculations require the calculation of the harmonic frequencies in the ground and the excited states, oscillator strengths, and non-adiabatic couplings. The evaluation of the integrals is not particularly expensive as it is based on analytical equations. The main computational cost is associated with the electronic structure calculation, and the most common methods are discussed in Section 3.2.

### 3. PES and the Restricted Access to a CI (RACI) Model

#### 3.1. Overview of the RACI model

A different view of AIE is obtained when the global potential energy surface (PES) is considered.<sup>[2,37]</sup> Figure 1 illustrates the issues that go beyond the assumptions of FGR theory. Although FGR provides insight into the coupling between the states in the neighborhood of the equilibrium geometries, relaxation in the excited state often involves the interaction between several states and can take the molecule far away from equilibrium. Low-frequency modes driving the photochemistry can be highly anharmonic, and non-adiabatic couplings in the equilibrium region do not necessarily correlate with the deactivation modes driving the photophysics or photochemistry.

The restricted access to a conical intersection (RACI) model<sup>[38]</sup> is based on the analysis of the PES topology and considers the important role of conical intersections (CI)<sup>[39–42]</sup> as funnels of electronic excitations. CIs are regions of the PES where the ground and excited states are degenerate and the probability of non-radiative internal conversion is maximal. Although they are frequently encountered far away from the Franck–Condon (FC) region (the ground-state equilibrium structure), as shown in Figure 1, they can be energetically accessible, in which case they become responsible for the rapid radiationless deactivation. In the RACI model, a CI is responsible for the decay in solution. However, in the aggregate phase, the energy of the CI increases owing to steric restrictions, blocking non-radiative deactivation pathways and enhancing the emissive response. The model provides information on the main non-radiative deactivation pathways connecting the FC region with the CI, and it does not carry any initial assumptions of the shape of the PES. As shown in Figure 2, the RACI model has been used to explain AIE in different kinds of systems including conjugated organic molecules,<sup>[1,38,43–47]</sup> boranes,<sup>[48]</sup> and excited-state proton transfer (ESIPT) molecules.<sup>[49,50]</sup> A similar picture is provided by excited-state dynamics calculations with trajectory surface hopping (TSH),<sup>[51]</sup> which directly simulate the decay to the ground state. This approach

has been applied to simulate the decay of diphenyldibenzofulvene (DPDBF)<sup>[52]</sup> and tetraphenylethylenes (TPEs).<sup>[44,53]</sup>

#### 3.2. Methodological considerations

The study of excited-state PES poses some challenges that make the choice of the method an important point. In principle, one possibility is to use multireference methods<sup>[54]</sup> such as CASSCF, which accounts for static correlation effects and is suitable to treat the energy degeneracy between the ground and excited states encountered at a CI. However, these methods have some limitations, namely the high computational cost and the need to define a set of active space orbitals. Choosing the active space is a problem because it should ideally cover all  $\pi$  orbitals of the molecule, but this is not practical for most AIEgens. In addition, multireference methods do not include dynamic correlation energy, although it can be complemented with CASPT2 or similar approaches to account for the latter effect.

Under these circumstances, a convenient alternative to explore the PES is provided by time-dependent density functional theory (TD-DFT),<sup>[55]</sup> which is more efficient computationally and allows for the treatment of large systems. TD-DFT has also been used as the electronic structure method in most FGR-based studies. It includes dynamic correlation energy and often gives a good account of the absorption and emission energies. However, the functional must be chosen with care, as some of the most usual functionals, like B3LYP, suffer from the so-called self-interaction error, which leads to the appearance of spurious CT states.<sup>[56]</sup> This error can be avoided by using long-range correlated functionals like CAM-B3LYP. The location of a CI with TD-DFT can also be problematic because they have highly distorted structures where the ground state acquires multireference character, which can cause TD-DFT to fail. Spin-flip (SF) TD-DFT,<sup>[57]</sup> where an “auxiliary” triplet state is used as the reference wave function, has been introduced to avoid this problem, but this method can also have problems owing to undesired spin contamination.

For the inclusion of environmental effects, these methods can be combined with a quantum mechanical/molecular mechanics (QM/MM) approach to include the crystal environment, or polarizable continuum methods to include bulk solvent effects. Although a detailed discussion of the methods used in the papers covered by this review is out of our scope, we will refer to the most relevant issues in the single cases, and we refer the reader to the original papers for more detailed discussions.

#### 3.3. Double bond torsion—DPDBF, styrene, and stilbene derivatives

The first molecule where the role of the CI in solution and aggregate phases was investigated is the prototypical AIEgen DPDBF (Figure 2).<sup>[58]</sup> An early TSH study using time-dependent Kohn–Sham and density functional tight binding predicted a lifetime of 1.4 ps in solution.<sup>[52]</sup> The lifetime increases by more than one order of magnitude in a locked derivative, and the

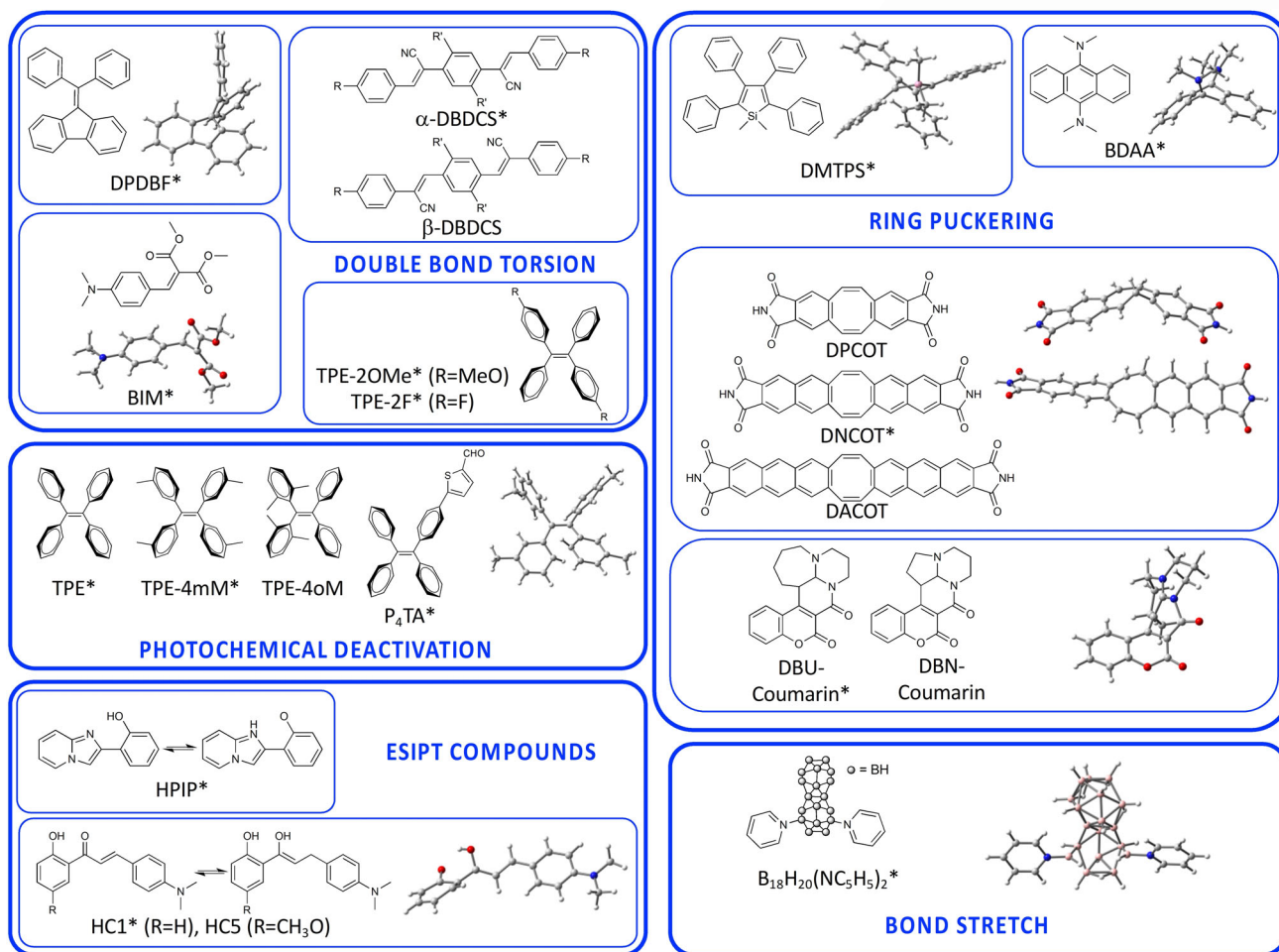


**Figure 2.** Overview of molecules discussed in section 3. AIEgens following the RACI model are labeled with an asterisk. The molecular models correspond to the CI structures responsible for radiationless decay in solution.

major contributions to the electronic non-adiabatic transition in DPDBF come from bond stretches in the DBF ring and ring rotation around the exocyclic double bond. The role of a CI in the decay was confirmed by MS-CASPT2//CASSCF calculations of the PES in solution and in the crystal (Figure 3).<sup>[43]</sup> Excited state relaxation in solution takes place mainly along two coordinates, the C–C stretch of the exocyclic double bond and torsion around it. The excited-state minimum,  $S_1$ -Min<sup>ac</sup>, has a significant twist angle of 59°, and an extended CI seam<sup>[59]</sup> can be found further along the C–C stretch and torsional coordinates. The minimum energy CI, ( $S_1/S_0$ )-CI<sup>ac</sup>, which has a twist angle of 90°, has an energy of 2.84 eV, lower than the excitation of 3.54 eV. Therefore, decay to the ground state is possible, explaining the lack of fluorescence in solution. The picture is consistent with that of parent fulvene,<sup>[60]</sup> showing that the fulvene unit plays the main role in the photophysics. In the crystal, rotation around the exocyclic double bond is hindered, and relaxation on  $S_1$  leads to a minimum with a torsion angle of 6°,  $S_1$ -Min<sup>crs</sup>. To reach the CI, the central bond has to stretch to 1.71 Å, and the energy increases to 4.83 eV, making the CI not accessible energetically.<sup>[61]</sup> This explains the appearance of fluorescence in the aggregate phase.

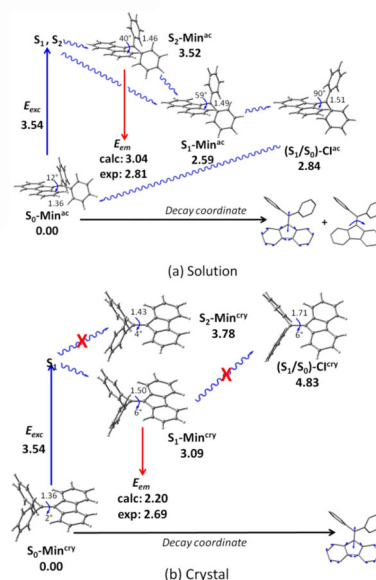


**Figure 3.** Calculated mechanisms for the photophysics of DPDBF in (a) acetonitrile and (b) the solid phase (crystal). Structural parameters: C–C distance of the exocyclic double bond and bond torsion angle. Straight blue and red arrows: excitation and emission. Curled blue arrow: vibrational relaxation and internal conversion. Energies in eV. Adapted from Ref. [43] with permission from The Royal Society of Chemistry.

The role of the phenyl substituents in the RACI model is different from that postulated in the FGR or RIM approaches. They do not act as “energy acceptors” that facilitate decay to the ground state but are responsible for the fact that rotation around the double bond is hindered in the crystal. Therefore, it can be anticipated that dibenzofulvene without the phenyl substituents will not be fluorescent in solution and will not show AIE, as rotation around the exocyclic double bond will not be restricted in the aggregate phase. The diphenyl substituents are also important to avoid stacked arrangements in the aggregate phase, which would lead to quenching.

Another AIEgen with a similar mechanism is 4-diethylamino-2-benzylidene malonic acid dimethyl ester (BIM), which contains a styrene unit (Figure 2).<sup>[62]</sup> Calculations combining TD-DFT, CASSCF, and CASPT2 show that the molecule in methanol solution relaxes, initially, to an excited-state minimum with FC-like structure,  $S_1$ -EM.<sup>[47]</sup> However, along the torsion coordinate of the styrene double bond there is a further  $S_1$  minimum,  $S_1$ -CT, and a CI,  $S_1/S_0$ -Clb, at 90° and 120° twist, respectively, where the excited state is a CT state from the benzene to the diester moiety (Figure 4). These structures are lower in energy

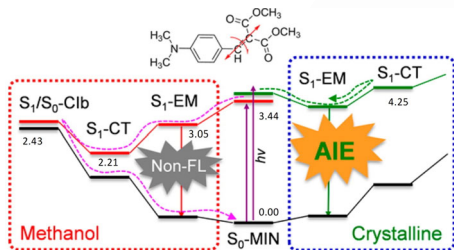


**Figure 4.** Schematic representation of the RACI mechanism in BIM, including relative energies in eV. Adapted with permission from Ref. [47]. Copyright 2016 American Chemical Society.

than the FC-like  $S_1$  minimum and the barrier to access them is very small, which suggests that the small fluorescence quantum yield in solution is due to decay through the twisted CI. The solvent polarity also plays an important role in the deactivation, as the CT state energy is lowered in methanol compared with the ground state. In the crystal, the rigid environment precludes the twist, and the molecule fluoresces from the FC-like minimum.

The RACI model also explains the different photophysics of a series of dicyano-distyrylbenzene (DBDCS) derivatives with two different CN substitution patterns ( $\alpha$  and  $\beta$  in Figure 2).<sup>[1]</sup> The compounds of the  $\alpha$  series have AIE behavior, whereas those from the  $\beta$  series are luminescent in solution and in the aggregate phase. Qualitative considerations based on the RIR and RIM models cannot explain this difference. However, TD-DFT and CASSCF calculations show that they are due to the energetic accessibility of a CI found along the torsion coordinate around one of the terminal double bonds. The energy profile around this coordinate is shown in Figure 5 for one member of each series where  $R = \text{BuO}$  and  $R' = \text{H}$  (Figure 2). The CI is found at a torsional angle of 90°. For the non-luminescent compounds in solution, the vertical excitation energy (2.9–

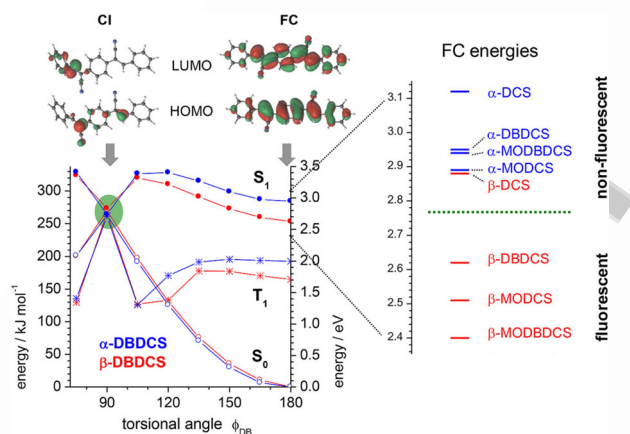


**Figure 5.** Left panel: TD-DFT rigid torsional scans ( $S_0$ ,  $S_1$ , and  $T_1$  energies) along a terminal double bond for  $\alpha$ -DBDCS and  $\beta$ -DBDCS. Top: CASSCF frontier HOMO- and LUMO-like orbitals characterizing the electronic structure for the CI and FC regions. Right panel: TD-DFT excitation energies calculated at the FC geometry in  $\text{CHCl}_3$ . Adapted with permission from Ref. [1]. Copyright 2017 American Chemical Society.

3.1 eV) lies above that of the estimated energy of the CI (2.8 eV), making the CI available for radiationless decay. In contrast, for the luminescent molecules, the vertical excitation energy (2.4–2.6 eV) lies below the CI energy, making the radiationless decay in solution not possible.

The fact that there are a variety of AIEgens carrying freely rotatable double bonds suggests that the RACI model may be quite general. For instance, it has been proposed that the RACI model explains the behavior of AIEgens based on 7,7'-diazaisoindigo,<sup>[34]</sup> which has two heterocyclic fragments joined by a double bond. However, there are no calculations on this system to support the idea. Another molecule that seems susceptible of decaying to the ground state through double bond rotation is TPE.<sup>[63]</sup> However, as we discuss in the next section, most TPE derivatives follow the RACI mechanism along a different coordinate.

### 3.4. TPE and its derivatives—Photocyclization vs. double bond torsion

TPE is another prototypical AIEgen (Figure 2),<sup>[63]</sup> and many derivatives have found AIE-related applications.<sup>[5]</sup> In spite of its similarity with the molecules from the previous section, parent TPE follows a different decay mechanism associated with formation of an interannular C–C bond. This was first shown in a TSH study, where 60 trajectories were run for up to 1.5 ps at the TD-DFT level. The majority of trajectories (75%) decay to the ground state through photocyclization, that is, formation of a C–C bond between adjacent phenyl rings. In a typical trajectory, decay to the ground state occurs at a CI with a C–C distance of 2.0 Å (Figure 6). Only 5% of trajectories decay to the ground state through the double bond rotation mechanism. The cyclization mechanism requires considerable displacement of the phenyl groups and is blocked in the aggregate phase. The theoretical prediction of cyclization has been recently confirmed by ultrafast transient absorption spectroscopy.

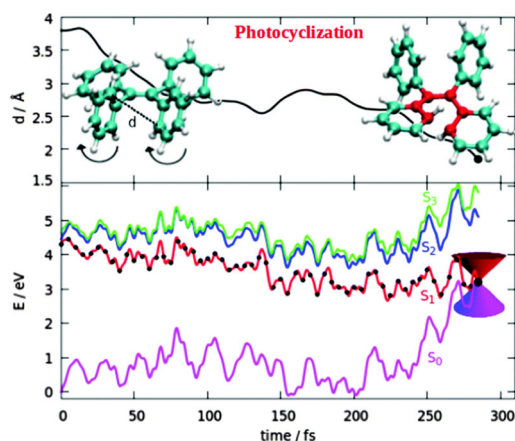


**Figure 6.** Interannular C–C distance (upper panel) and electronic state potential energies (lower panel,  $S_0/S_1/S_2/S_3$  shown in magenta/red/blue/green) as a function of time for a representative trajectory undergoing photocyclization. The actual (running) electronic state is shown in black. All the energies are relative to the initial (0 fs) energy. Initial (0 fs) and final (close to the CI) molecular structures are shown. Trajectories computed at the PBE0/def2-SVP level. Adapted from Ref. [53] with permission from the PCCP Owner Societies.

copy<sup>[64]</sup> where the cyclized intermediate is observed approximately 20 ps after excitation. It has a lifetime of 159 s and could be isolated as a phenanthrene derivative after oxidation, confirming the photocyclization mechanism.

A similar AIE behavior is followed by a tetramethylated derivative carrying the methyl groups in *meta* position, TPE-4mMe. This is shown by gas-phase calculations combining the semiempirical OM2/MRCI level with CASSCF and CASPT2. Four CIs have been located for this molecule, two along the cycloaddition and two along the double bond torsion route. The CIs for cycloaddition,  $CI_{cyc}$ , are connected to the FC geometry by a barrierless path at the OM2/MRCI level (Figure 7, left panel). Consistent with this, 88% out of 558 TSH calculations run during 1 ps decay to the ground state through  $CI_{cyc}$ . The OM2/MRCI energy picture is confirmed by CASPT2, and the computations are consistent with the ultrafast spectroscopic study of Ref. [64], where TPE-4mMe has similar dynamics to TPE. In contrast, TPE-4oMe, which has four methyl groups in the *ortho* position, is strongly fluorescent in solution. Calculations indicate that this happens because of sizeable barriers (0.3–0.4 eV) to access the CI (Figure 7, lower panel), and no decay to the ground state is observed for 568 TSH trajectories run for 1 ps. This is also consistent with the spectroscopic study,<sup>[64]</sup> where the time constant determined for TPE-4oMe cyclization and decay to the ground state is 4.07 ns, much longer than the simulation timescale.

Another TPE-based AIEgen that has been suggested to follow the RACI model is 5-(4-(1,2,2,triphenylvinyl)-phenyl)thiophene-2-carbaldehyde (P<sub>4</sub>TA)<sup>[65]</sup> (Figure 2), where a CI along the cyclization coordinate has been also located at the TD-DFT level.<sup>[32]</sup> FGR calculations are consistent with this picture and suggest that the deactivation is promoted by the twisting vibration of the phenyl rings, which brings the rings together.

The behavior of TPE-2OMe and TPE-2F,<sup>[66]</sup> which have methoxy or fluoro substituents on two phenyl groups lying on

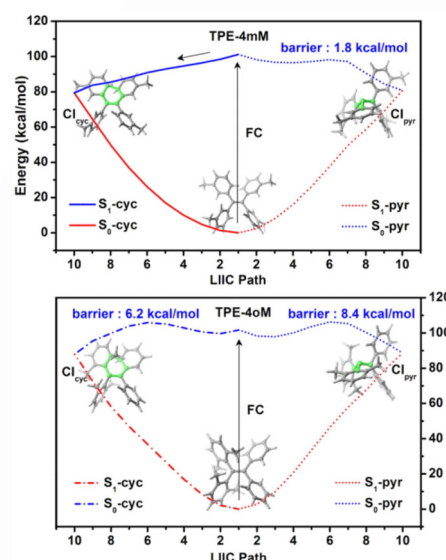


**Figure 7.** OM2/MRCI-computed LIIC paths connecting the FC points and the  $S_1/S_0$  CI related to the cyclization and photoisomerization of TPE-4mMe (upper panel) and TPE-4oMe (lower panel). Adapted with permission from Ref. [44]. Copyright 2017 American Chemical Society (ACS). Further permissions related to this material should be related to the ACS.

opposite sides of the central double bond (Figure 2), is different from the TPE derivatives discussed up to now. Experiments show that these AIEgens undergo photochemical *E–Z* isomerization, and TD-B3LYP calculations show that the excited-state steepest decay path from the FC structure leads to  $S_1$  minima with nearly perpendicular configuration (90° twist around the central double bond) and an  $S_1–S_0$  gap of only 0.5 eV, suggesting that there is a CI nearby (Figure 8). Thus, these molecules seem to follow the RACI model associated with double bond torsion. Overall, the results for the TPE derivatives suggest that this group of compounds can, in principle, decay to  $S_0$  in solu-

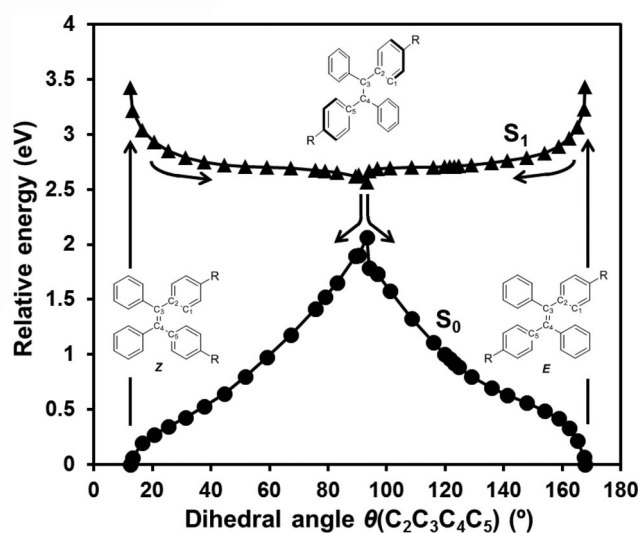


**Figure 8.** TD-B3LYP excited-state steepest descent paths from the Z and E FC points of TPE-2OMe. The horizontal and vertical axes correspond to the  $\pi$  twist angle and the relative energy, respectively. Reprinted with permission from Ref. [66]. Copyright 2018 American Chemical Society.

tion along the photocyclization and double bond torsion coordinates. The preference for one or the other decay mechanism or the appearance of fluorescence in solution depends on the barriers found along the different paths, which in turn will depend on steric and electronic characteristics of the substituents.

### 3.5. Ring puckering—dimethyl tetraphenylsilole (DMTPS), 9,10-bis-(*N,N*-dimethylamino)anthracene (BDAA), cyclooctatetraene (COT), acenimides, and $\pi$ -extended coumarins

Phenyl-substituted siloles are the first group of compounds where AIE was identified.<sup>[3,28,67]</sup> The PES obtained for the representative DMTPS molecule (Figure 2) from combined TD-DFT, CASSCF, and CASPT2 calculations (Figure 9) shows that it also follows the RACI model.<sup>[38]</sup> Excited-state relaxation in solution

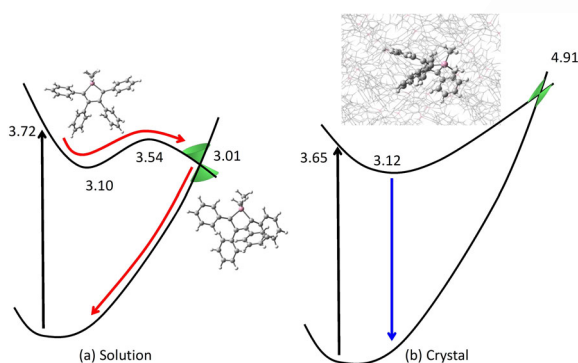


**Figure 9.** Summary of the proposed decay paths of DMTPS in (a) solution and (b) in the crystal. Adapted from Ref. [38] with permission from the Royal Society of Chemistry.

leads to a FC-like  $S_1$  minimum at 3.1 eV where the silole ring keeps a nearly planar structure. The PES has a CI at 3.0 eV, which is separated by a barrier with an estimated energy of 3.54 eV, smaller than the vertical excitation energy of 3.72 eV. The CI is characterized by ring puckering and a flapping motion of the phenyl substituents. Mechanistically, the arrangement of the four C atoms is similar to that found for one of the CIs of *cis*-butadiene.<sup>[68]</sup> The energetically accessible CI explains the lack of fluorescence in solution. In the crystal, radiationless decay is disfavored because the volume-requiring coordinate is hindered and an energy of 4.91 eV is required to reach the CI.

Another AIEgen that follows the RACI model along a ring puckering coordinate is BDAA (Figure 2).<sup>[45]</sup> TD-B3LYP calculations show that there is a CI on the PES responsible for the lack of fluorescence in solution. It has a relative energy of 3.84 eV at the CASSCF level, lower than the vertical excitation of 4.32 eV. The CI is characterized by a boat-like conformation of the central anthracene ring, with the two bulky amino substituents coming out of the plane (Figure 2). It has a quinoid biradical character in the central ring and is reminiscent of Dewar benzene, similar to one of the structures found in the CI seam of benzene, of  $C_{2v}$  symmetry.<sup>[69]</sup> Although the photo-physics in the crystal have not been studied, it is postulated

that the large displacements required to reach the CI will not be feasible in the crystal phase, which explains the appearance of luminescence.

The role of CIs involving a ring puckering coordinate also seems to be important in the radiationless decay of three similar acenimides with different luminescent behavior. These are three conjugated systems consisting of a COT core and diphenylene, dinaphthalene, and dianthraceneimide wings (DPCOT, DNCOT, and DACOT, see Figure 2).<sup>[70,71]</sup> Their PES has been studied with SF-TD-DFT calculations combined with the global reaction route mapping (GRRM)<sup>[72,73]</sup> strategy.<sup>[46]</sup> DNCOT has AIE behavior and is V-shaped in the ground state because of the boat-like COT structure (Figure 10, left panel), with the wings

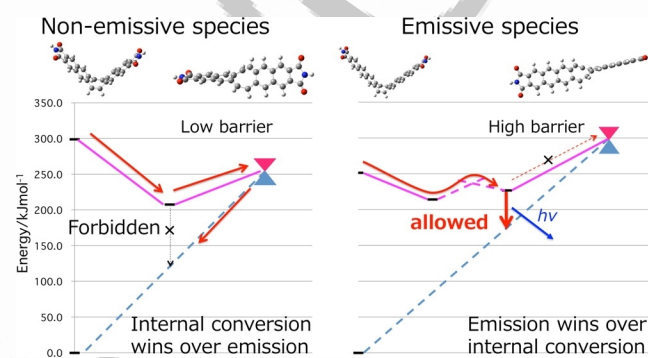


**Figure 10.** Schematic representation of the mechanisms governing AIE in DNCOT (left panel) and emission in solution in DACOT (right panel). Reproduced with permission from Ref. [46]. Copyright 2015 American Chemical Society (ACS). Further permissions related to this material should be related to the ACS.

attached to the two raised sides of the cycle. The vertical excitation energy is 3.10 eV, and relaxation on  $S_1$  leads to a planar minimum at 2.15 eV. On the PES, there is a CI with a pseudo-tub-shaped COT conformation, with the naphthaleneimide wings attached on the sides, which has an energy of 2.75 eV. This CI is energetically accessible in solution and has large steric requirements that make it not accessible in the aggregate phase, consistent with the RACI model. As for the other derivatives, the results suggest that DPCOT is not fluorescent in the aggregate phase because it can decay through a different CI, which involves a volume-conserving coordinate, an out-of-plane bending of two CH bonds on the COT ring. In contrast, DACOT is fluorescent in solution because the CI found for that molecule is too high in energy (Figure 10, right panel). Overall, the mechanism proposed for these acenimides is in good agreement with experiment, but it should be noted that the calculations have some limitations inherent to the SF-TD-DFT approach. Some of the structures show significant spin contamination owing to spurious singlet–triplet mixing, and calculations at a higher level of theory are necessary to confirm the mechanistic picture.

Similar ideas are useful to understand the behavior of a series of  $\pi$ -extended coumarins, derivatives of 3*H*-chromeno[3,4-*c*]pyridine-4,5-diones (Figure 2).<sup>[75]</sup> The compounds originating from condensation with 1,8-diazabicyclo[5.4.0]undec-7-ene (DBU), which have saturated six- and seven-membered



rings attached to the pyridone ring, show AIE behavior. TD-DFT calculations on a representative derivative in  $\text{CH}_2\text{Cl}_2$  (Figure 11) show that the lack of fluorescence in solution is due to internal conversion at a distorted structure where the central pyridone ring is puckered and the  $S_1$ - $S_0$  energy gap is about 0.5 eV in the gas phase and 0.3 eV in solution. This structure is separated from the FC region by a barrier of approximately 0.2 eV, and we would speculate that there is a CI in its vicinity responsible for the decay. Similar to BIM, the solvent reduces the  $S_1$ - $S_0$  gap and favors internal conversion because the  $S_1$  state has a partial CT from the pyridinone to the chromene. Calculations on dimers embedded in the crystal show that the packing reduces the possibility of deformation of the seven-membered ring and hinders radiationless decay. In contrast, the compounds derived from DBN, which have a five-membered instead of a six-membered ring attached to the pyridone, are luminescent in solution because formation of the distorted  $S_1$  minimum is not possible owing to the restriction imposed by the more rigid, smaller ring.

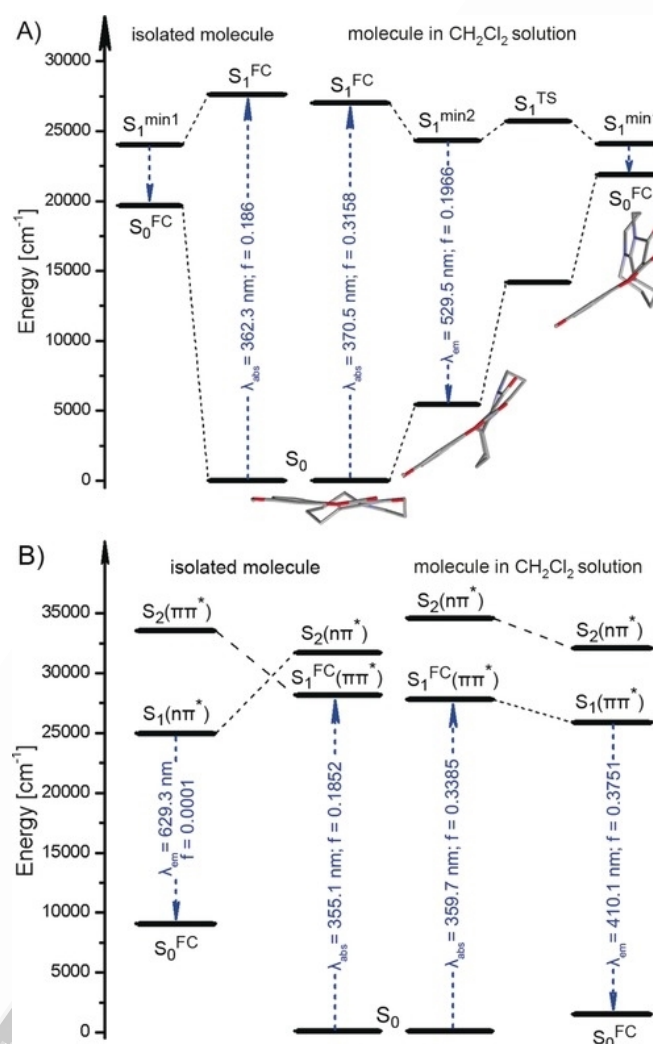


**Figure 11.** Energy diagram for a  $\pi$ -extended coumarin condensation compound with DBU. The energy of the molecule at the FC structure is defined as zero reference energy. Reprinted from Ref. [74] with permission from John Wiley and Sons.

### 3.6. ESIPT compounds—Hydroxyphenylimidazopyridine (HPIP) and 2'-hydroxychalcones (HC)

Excited-state intramolecular proton transfer (ESIPT) compounds form a broad group of AIEgens where the absorbing and emitting species are different owing to the occurrence of fast ESIPT before emission.<sup>[5]</sup> In contrast to the AIEgens discussed previously, which do not undergo aggregation quenching because they have bulky substituents that prevent stacking, ESIPT AIEgens are often planar. The quenching is prevented because the excitation localizes spontaneously on the molecule that undergoes ESIPT, which usually has a lower excitation energy than the surrounding molecules. In this way, the formation of non-emissive delocalized states is avoided.

HPIP (Figure 2) has raised great interest because of its unusual solid-state photophysics, which have been reviewed recently.<sup>[76]</sup> The luminescence of HPIP crystals comes from the keto form, which is formed after ESIPT from the enol ground state. HPIP is the first AIEgen where the involvement of a CI was invoked to explain the lack of fluorescence in solution, combining TD-DFT and CASSCF calculations (Figure 12).<sup>[50]</sup> After

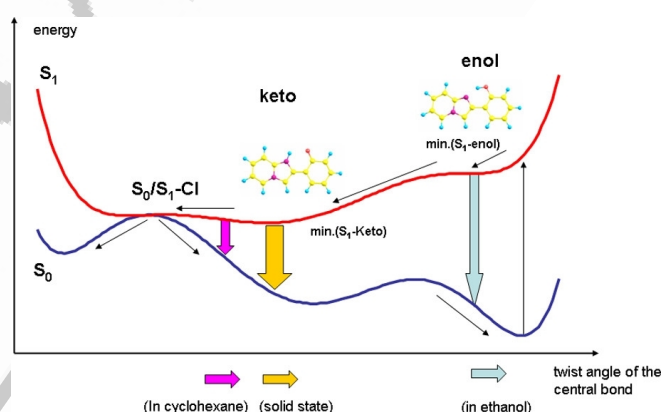


**Figure 12.** Schematic potential energy surface for AIE behavior of the keto form of HPIP (orange and magenta arrows). The blue arrow represents fluorescence from the enol form observed in ethanol. Reproduced with permission from Ref. [50]. Copyright 2012 American Chemical Society.

excitation of the enol ground state, the molecule relaxes on  $S_1$  and yields the keto form. Importantly, torsion around the central bond in the keto form leads to a CI between the excited and the ground state, as shown by CASSCF calculations, which is reminiscent of similar CIs found for other ESIPT compounds.<sup>[77,78]</sup> The CI is separated from the minimum by a small barrier, and this explains the radiationless decay and the lack of fluorescence observed in the ground state. In the crystal, the torsion is blocked, and the molecule emits.

Another ESIPT AIEgen where a CI lies behind the lack of fluorescence in solution is a 2'-hydroxychalcone derivative (HC1, Figure 2).<sup>[49,79]</sup> The PES for this molecule has been studied recently together with the effect of electrostatic interactions on the non-radiative rate in the solid phase. The results are presented in Section 4.2 in the context of intermolecular effects.

### 3.7. Bond stretch— $B_{18}H_{20}(NC_5H_5)_2$ cluster

Boranes and carboranes are another group of AIEgens, and the role of a CI in the radiationless decay has been recently demonstrated for the  $B_{18}H_{20}(NC_5H_5)_2$  cluster,<sup>[48]</sup> which is composed of two conjoined boron hydride subclusters bearing two pyridine substituents. The AIE behavior is explained with the global PES calculated at the CASPT2//CASSCF level (Figure 13).

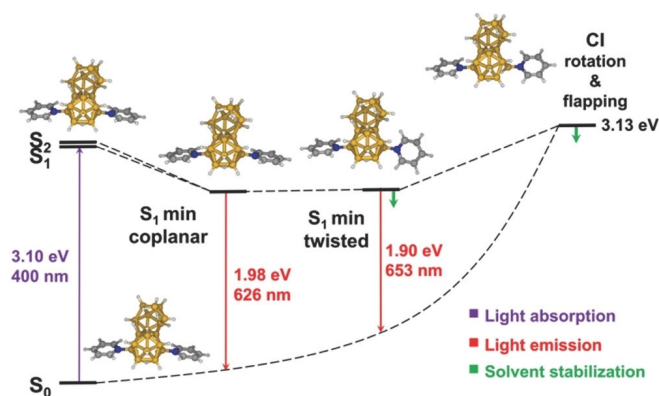


**Figure 13.** Scheme of  $B_{18}H_{20}(NC_5H_5)_2$  photophysics based on CASPT2//CASSCF computations. Reprinted from Ref. [48] with permission from John Wiley and Sons.

At this level of theory, the calculated vertical excitation is 3.10 eV. Relaxation on  $S_1$  can lead to two minima, one where the orientation of the pyridine groups is similar to that in the ground state minimum and another one where the rings are twisted. In addition, a CI can be found at 3.13 eV, almost isoenergetic with the vertical excitation energy. It is characterized by a rotation and flapping motion of the pyridine rings, which induces significant stretching of the two B–B bonds from 1.848 and 1.973 Å at the FC structure to 2.194 Å and 2.492 Å. The radiationless decay in solution is enhanced at the energetically accessible CI, leading to weak emission. Radiationless decay is accelerated in strongly polar solvents like DMF or DMSO, where no emission at all is visible, because the excited state at the CI has a pronounced CT character from one of the pyridine rings to one of the semidissociated boron atoms, and the CI energy is lowered through stabilization of the excited state by the polar solvent. The large distortion required to access the CI is blocked in the solid state, and this explains the appearance of AIE.

### 3.8. The RACI and FGR models—Differences and complementarities

The RACI and FGR models have different but complementary underlying assumptions. In FGR,  $k_{nr}$  is determined by two components, corresponding to the coupling of the nuclear and electronic wave functions through the vibrations. For the nuclear part, the FGR approach usually relies on the harmonic approximation, where nuclear changes induced by the excitation are described in terms of displacements along vibrational

modes described with a harmonic potential. This is a suitable approach when the geometry changes induced by the excitation are small, and for vibrations that have only a small effect on the energy, such as phenyl group rotations frequently encountered in AIEgens. Further modifications of the theory including anharmonic PES can help extend the application of these methods. However, FGR is not suitable to treat large nuclear distortions such as the ones that lead to a CI, which involve highly anharmonic potentials and large changes in the electronic coupling, and it cannot predict  $k_{nr}$  reliably. In these cases, a better description is provided by the RACI model, which is focused on the PES and the electronic coupling at the CI. When a CI is involved, predictions of the excited-state lifetimes in solution require dynamics calculations by using TSH or similar approaches. In the aggregate phase, the situation is different because the harmonic approximation is often valid thanks to the steric restrictions imposed by the environment. In this case, FGR can provide good estimates of the lifetimes, as proved by its success in describing AIEgen properties in the solid state.<sup>[10,13]</sup> Therefore, the two approaches are complementary: the RACI model is useful to determine the modes that are responsible for radiationless decay in solution, as the short excited-state lifetimes are often associated with decay at the CI; and the FGR approach is useful for a quantitative treatment of lifetimes in the aggregate phase.

## 4. Effect of Intermolecular Interactions and the Environment

Another important issue is the role of electronic intermolecular interactions. The initial research on AIEgens focused on siloles and propeller-shaped compounds where the effect of exciton formation is minimal.<sup>[8,16,22,25,26,33,80]</sup> Consequently, it has been assumed that in the mechanism of AIE, the environment acts as a perturbation to the excited states of a central molecule. Most simulations of AIEgens follow this idea and use QM/MM methods where only one molecule is included in the QM region. Consequently, only the steric effects associated with the short-range coulombic interactions with the MM regions are considered and quantum terms such as electron exchange and intermolecular charge transfer are not taken into account. However, specific interactions, long-range electrostatics, and exciton effects can affect the energetics of the excited states and their transition probabilities. In fact, some authors have claimed that the term AIE should be reserved for cases involving intermolecular electronic interactions, whereas the cases involving steric confinement should be classified as solid-state enhanced emission.<sup>[1]</sup> In any case, the significant role of the environment can be illustrated with several examples in the solid state, where small changes of the electronic structure by substitution, or changes in the relative orientation of neighboring molecules such as in polymorphic crystals lead to distinctive emissive properties from aggregation quenching to AIE.<sup>[1,49,81,82]</sup> A better understanding of the interplay between intermolecular and intramolecular forces, as well as electronic versus steric effects, is essential to understand AIE in depth.

#### 4.1. H versus J aggregation

In the condensed phase, both  $k_r$  and  $k_{nr}$  are modulated by the environment. To reduce  $k_{nr}$ , non-radiative pathways should be hampered. Some common strategies to achieve this involve increasing optical gaps and the rigidification of the molecules and environments.<sup>[1]</sup> In terms of the intermolecular factors,  $k_r$  can be enhanced by increasing the prevalence of J-aggregates, efficient Herzberg–Teller coupling, and dense unit cells. Dense packing and monolithic crystals can also help decrease  $k_{nr}$ .

The relative orientation of the chromophores is important to understand the effect of excitonic coupling on the photophysics of aggregates.<sup>[83,84]</sup> According to the Kasha exciton model, stabilization of J-dimers with head-to-tail alignments of the transition dipole moments ( $\mu$ ) shifts absorption to the red whereas the oscillator strength of  $S_1$  is twice that of the isolated molecules (Figure 14).<sup>[85]</sup> This is in contrast with H-dimers (side-to-side arrangements of  $\mu$ ) where the absorption is blue-shifted and emission is forbidden. The energy splitting resulting from aggregate formation depends on exciton couplings ( $J_{AB}$ ). Nevertheless, these models are based on strong approximations that can break down in molecular crystals and concentrated solutions, where coulombic interactions amongst all molecular units should be accounted for.<sup>[1]</sup> Additionally,  $\Phi_f$  does not only depend on  $k_r$ , but also on the competition with the non-radiative pathways  $k_{nr}$ .<sup>[86]</sup> As a result, H-aggregates can show significant emission in the condensed phase.<sup>[1,87]</sup> A recent review by Hestand and Spano describes recent developments of the Kasha model including the effect of CT states and vibronic couplings.<sup>[88]</sup>

Gierschner et al. have thoroughly investigated the effect of substitution in all-*trans* *para*-distyrylbenzene (DSB) crystals.<sup>[1,89]</sup> DSB can be crystallized into two polymorphic forms: plate-like and needle-like structures.<sup>[86]</sup> Both forms contain H-type aggregates in herringbone arrangements and show significant quantum yields (65% and 78%, respectively). By using a combination of experiments and modeling, the authors have systematically analyzed two series of DSB crystals ( $\alpha$  and  $\beta$ , Figure 15), showing enhanced luminescence in the solid state. Most of

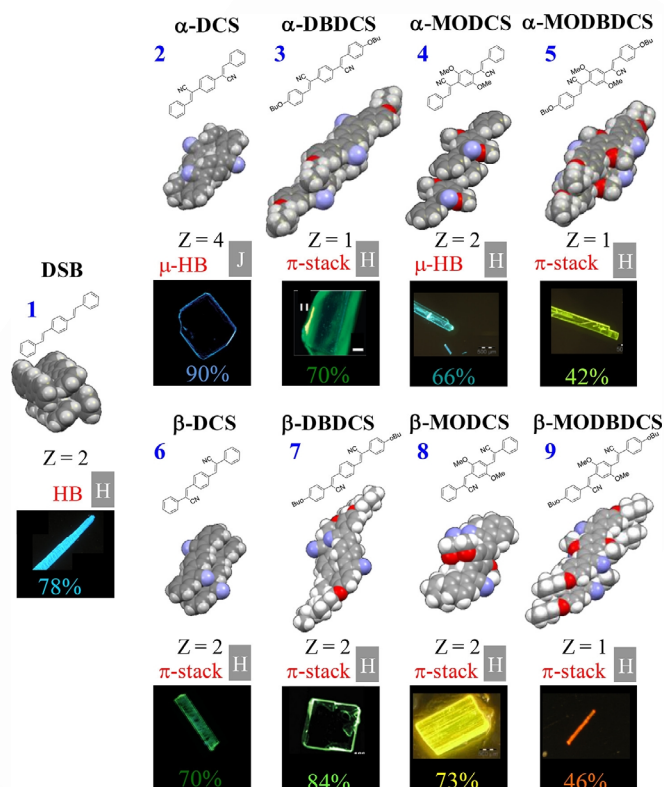


**Figure 15.** Quantum efficiencies and features of the crystal structures for the series  $\alpha$  and  $\beta$  of DSB derivatives investigated in Ref. [1]. Relevant features of the crystal structure including dominant arrangements (HB: herringbone and  $\pi$ -stacking) and the dominant couplings are specified (H vs. J couplings). Adapted with permission from Ref. [1]. Copyright 2017 American Chemical Society.

these crystals contain H-aggregates and are stabilized by  $\pi$ -stacking interactions. Both features are normally associated with a decrease of  $k_r$  and aggregation quenching, but the crystals still show enhanced emission. The reason for this is associated with the restriction of non-radiative mechanisms in the densely packed environment that forces planarization of the molecules (see also section 3.3). Consequently, the  $k_{nr}$  values for all these crystals are significantly smaller than in solution.

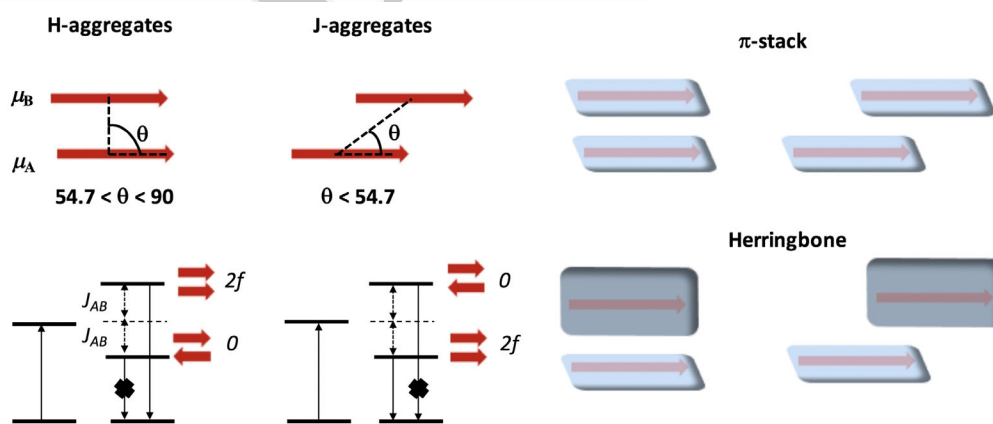


**Figure 14.** Illustration of the orientation of the transition dipole moments ( $\mu$ ) for J- and H-aggregates. For the H-aggregates, emission is forbidden (oscillator strength,  $f=0$ ), whereas for J-aggregates the transition dipole moment is twice the value of the molecule ( $2f$ ). On the right,  $\pi$ -stacked and herringbone configurations in dimers of planar aromatic molecules are illustrated.

1 Within the FGR-RIM scheme, Shuai et al. have considered the  
2 effect of including exciton couplings on the calculation of  
3  $k_{nr}$ .<sup>[24]</sup> Based on the investigation of typical AIEgens with relatively  
4 small couplings ( $0.2 < |J_{AB}| < 27.1$  meV), the authors concluded that the  
5 exciton couplings have a minor effect on the  $k_{nr}$  values. However, regardless  
6 of the prevalence of H or J aggregation, the value of  $k_{nr}$  always increased  
7 with the value of the coupling. Taking into account that the couplings depend  
8 on the overlap between the molecules, crystals with low packing  
9 densities should help avoid exciton effects. Nonetheless, compact crystals  
10 help restrict intermolecular rotations, force planarity (which increases  $k_r$ ),  
11 and avoid alternative non-radiative pathways. The balance between these  
12 competing factors will determine whether a crystal will enhance or quench  
13 fluorescence in the solid state.

14 Polymorph-dependent luminescence has been studied for 6-CN-HPIP,  
15 a molecule that undergoes ES IPT. This HPIP derivative (Figure 2) has  
16 three polymorphs that fluoresce with different colors.<sup>[90]</sup> The color of the  
17 emission is the result of different factors. First, the main effect comes from  
18 the molecules that are directly stacked with the emitter rather than from the  
19 overall surroundings. Second, the shifts in the emission energies come from  
20 the fact that the emitter is the keto form of 6-CN-HPIP surrounded by enol  
21 molecules with opposite dipole moment. Third, the energy shifts are very  
22 sensitive to environment; face-to-face and side-to-side interactions induce,  
23 preferentially, bathochromic and hypsochromic shifts, respectively.<sup>[82]</sup> Overall,  
24 these studies show that the emission color is very sensitive to environment,  
25 making it difficult to predict.

## 4.2. Effect of electrostatic interactions

26 Short- and long-range electrostatic interactions can also affect the balance  
27 between radiative and non-radiative mechanisms. One example is the case of  
28 2'-hydrochalcone derivatives (Figure 16).<sup>[49,91]</sup> There are two non-radiative  
29 competing processes that involve intramolecular rotation in the enol (E) and  
30 keto (K) forms.<sup>[49]</sup> Both mechanisms take the molecules to the ground state  
31 through the CI, which are accessible in vacuum. Non-adiabatic dynamics  
32 simulations have shown that the rela-

33 tive population of these reaction channels is controlled by the substituent  
34 with a splitting of 48.52 (E/K) for HC1 versus 80:20 for HC5. The bias toward  
35 the proton transfer mechanism found for HC5 is related to the significant  
36 stabilization of the keto form. In the solid state, although HC1 shows  
37 significant J aggregation featuring herringbone dimers, HC5 shows mainly  
38 H aggregation with  $\pi$ -stacking dimers (Figure 16). However, aggregates  
39 of HC5 have significant oscillator strengths and the aggregation quenching  
40 of HC5 cannot be explained by only considering radiative pathways. Because  
41 the distortion is restricted in the crystal, the deactivation through the enol  
42 channel is hampered in both cases; however, the keto channel is only  
43 restricted for HC1.<sup>[92]</sup> The accessibility of non-radiative mechanisms in the  
44 crystal environment explains the quenching of fluorescence in HC5, which  
45 is driven by electrostatic interactions that help stabilize the CI in the solid  
46 state.

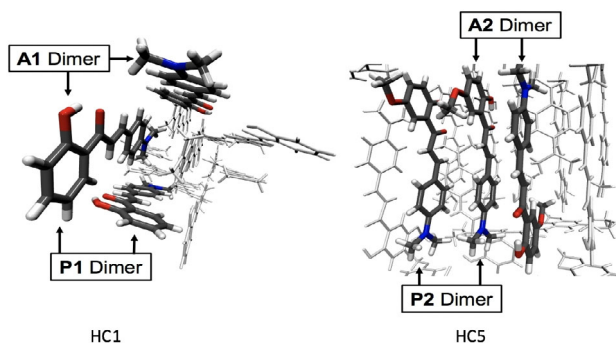
47 Interestingly, in the context of the FGR-RIM model, Ma et al. found that  
48 electrostatic interactions enhanced the rate constants for the  $T_1$ - $S_0$  radiative  
49 decay in crystals of dicarboxylic acids, but they can also decrease the  
50 radiative decay.<sup>[93]</sup> In another recent investigation, Presti et al. considered  
51 the reasons behind AIE in crystals of 2,7-diphenylfluorene.<sup>[94]</sup> In contrast  
52 with the previous interpretation of the emission mechanism based on the  
53 formation of excimers, the authors found that the enhancement of the  
54 fluorescence was associated with the electrostatic interactions with the  
55 central molecule increasing the radiative decay rate.

## 4.3. Effect of amorphization

56 Moving from the crystalline to the amorphous phase also has an effect on  
57 the emissive response.<sup>[26,95]</sup> In a recent investigation using the FGR-RIM  
58 model, embedded and exposed molecules in amorphous nanoparticles of HPS  
59 with different sizes were considered (Figure 17).<sup>[26]</sup> The average  
60 reorganization energies ( $\lambda$ ) of embedded molecules are size independent  
61 and similar to those of the crystal, whereas for the exposed molecules,  
62 the values are closer to those obtained for the isolated molecule in the  
63 gas phase. The quantum efficiencies of embedded molecules do not depend  
64 on the size of the particles and have  $\Phi_f > 92.7\%$ , similar to the value for  
65 the crystal ( $\Phi_f = 97.9\%$ ). In contrast, the exposed models have very small  
66 efficiencies with values in the range 0–6.43%.

## 4.4. Alternative mechanisms

67 An alternative to exciton formation between aggregates is intermolecular  
68 CT, which has been postulated to be responsible for the appearance of  
69 luminescence in a supramolecular hydrogel based on 1,3,5-benzene  
70 trisamide (BTA; Figure 18).<sup>[96]</sup> TD-DFT calculations with the B3LYP  
71 functional indicate that the excited-state energy ( $S_1$ ) decreases gradually  
72 on going from the monomer (3.8 eV) to the dimer, trimer, and tetramer  
73 (3.3, 2.7, and 2.5 eV, respectively), which is consistent with the redshift  
74 observed experimentally when the degree of aggregation increases. The  
75  $S_1$  state is postulated to have a strong CT from the peripheral groups to  
76 the benzene cores and low oscillator



77 **Figure 16.** Arrangements of dimers in molecular crystals of HC1 and HC5. Adapted with permission from Ref. [92]. Copyright 2017 American Chemical Society.

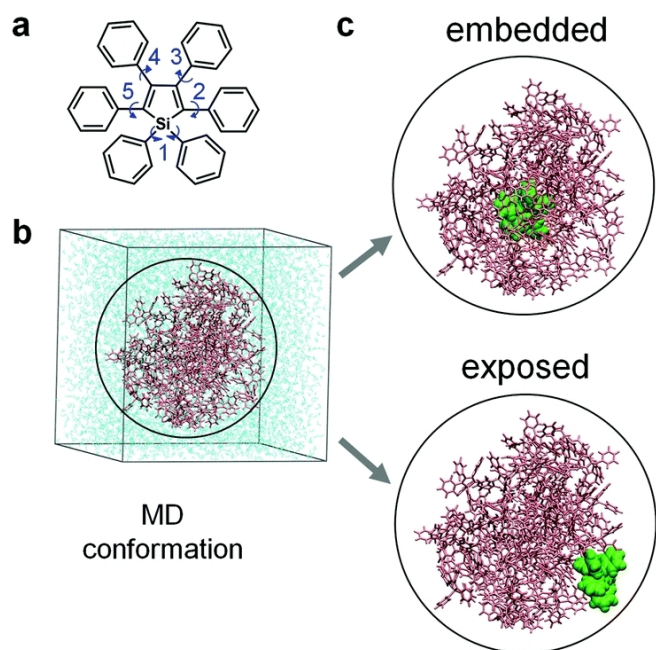


**Figure 17.** Nanoparticle models with the HPS molecule embedded or exposed to the solvent. Adapted from Ref. [26] with permission from the Royal Society of Chemistry.

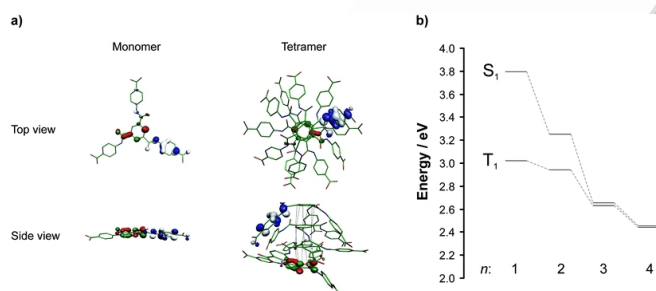


**Figure 18.** HOMO (blue/white) and LUMO (red/green) orbitals for the monomer and tetramers of BTA. Energies of singlet and triplet excited states with the number of molecules in the aggregates. Reproduced from Ref. [96] with permission from the Royal Society of Chemistry.

strength. It would be desirable to confirm these results with a long-range correlated functional (see section 3.2), as the B3LYP functional is known to underestimate the energy of CT states.

A different mechanism from those discussed until now, namely changes in *intramolecular* through-space coupling upon aggregation, has been proposed to be behind the “unconventional” visible-light luminescence in molecules with peripheral phenyl groups.<sup>[97,98]</sup> Combining experimental techniques and (TD)-DFT calculations, the authors suggested that the AIE of these compounds is due to the formation of *intramolecular*<sup>[97,98]</sup> and *intermolecular*<sup>[98]</sup> through-space dimers (Figure 19). The interpretation was based either on the analysis of the reorganization energies or the geometries of S<sub>1</sub>. Overall, these calculations support the picture that intramolecular through-space coupling leads to the redshift observed upon aggregation, but more sophisticated calculations are required to provide a mechanistic interpretation of these processes.

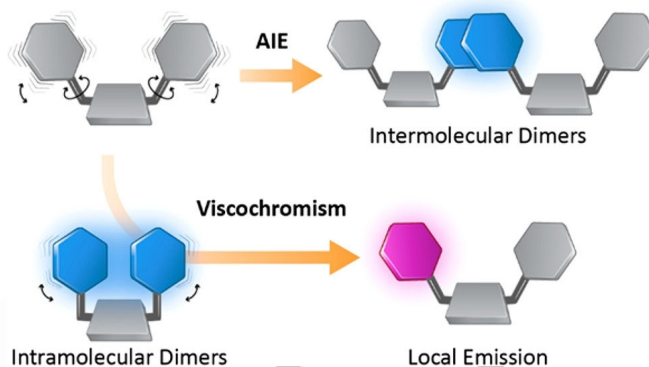


**Figure 19.** Scheme of the two processes proposed to explain luminescence in phenyl-ring molecular rotors. Reproduced with permission from Ref. [98]. Copyright 2017 American Chemical Society.

## 5. Conclusions and Perspectives

AIE is a very fertile ground for the design of luminescent materials, and it has reached an impressive range of technological applications in areas such as bioimaging, detection, visualization techniques, and OLEDs. Today’s research in the field aims at expanding these applications and developing more efficient AIEgens. Theory has played an important role in our understanding, uncovering the molecular mechanisms behind the photophysics in solution and in the aggregate phases—FGR is a powerful approach for the quantitative treatment of luminescence in the aggregate state, whereas the study of PES and the RACI model have discovered the reasons behind the lack of fluorescence in solution for several representative AIEgens. It is clear that the RACI model will not be applicable to all AIEgens because the lack of fluorescence in solution may also be due, for example, to classical internal conversion as described by the FGR approach. Other mechanisms such as restriction of long-range energy transfer in the aggregate phase may also play a role. Still, the number and variety of current examples suggest that the RACI model must be quite general. The fact that most CIs described up to now for AIEgens are related to previously known CIs of other molecules should also be useful to rationalize the photophysics of other AIEgens.

In spite of this success, there are still challenging questions for theory and computations. At the molecular level, this includes phenomena such as clusteroluminescence<sup>[99]</sup> or luminescence from non-conventional chromophores,<sup>[100–102]</sup> which are not well understood yet. In this context, ultrafast spectroscopy is another tool that can also provide important contributions to the molecular-level understanding of AIE. The recent study on TPE derivatives<sup>[64]</sup> is an example of how, together with theory, it can help us to understand the fundamental behavior. If these types of studies are extended to other AIEgens, one can expect that similar synergies will appear as those that have led to a thorough understanding of the photophysics of DNA components, to name a successful example.<sup>[103]</sup> Reaching such a detailed level of understanding should be one of the main goals of fundamental AIE research today.

Another issue where our understanding has to be improved concerns the role of intermolecular interactions and the environment in aggregate and solid phases. The examples described above illustrate that they modulate the radiative and non-radiative mechanisms and the color of emission. However, this depends on many factors. Depending on the crystal structure, localized or delocalized exciton states will prevail. In addition,  $\pi$ - $\pi$  interactions can lead to quenching but also to enhanced luminescence. Electrostatic interactions can modulate the CI energy, determining whether radiationless decay in the aggregate phase is favored or not. Overall, the final effect in terms of  $\Phi_f$  and emission color depends on multiple factors and is challenging to predict. Therefore, advances on this subject will require the use of computational methods that are sufficiently accurate to treat the interactions. Another possibility to treat intermolecular interactions in crystals is to use periodic DFT, which to our knowledge has not been applied yet to study AIE. For instance, a recent development by Saita et al. describes a method to explore ISC pathways by using DFT periodic boundary conditions considering gradient projection and single-component artificial-force-induced reaction algorithms.<sup>[104]</sup> This and similar developments shall open up new alternatives for the study of AIE in the solid state.

A further issue that deserves more attention from theory is amorphous aggregates. Although there are several examples in crystalline environments, the calculation of the photophysics of amorphous aggregates, for example, for nanoparticles formed in poor solvents, has been addressed less frequently. The QM/MM study of Ref. [26] is a promising step in this direction, which will provide new understanding of the way that aggregation modulates the color of fluorescence or a phenomenon such as morphochromism.

A final challenge for theory is to model the photophysics of AIEgens in their application media. For instance, modeling of AIEgenic biological probes embedded in their biological environments should be possible by using similar QM/MM techniques to those used for the study of crystals or aggregated nanoparticles. This will increase the impact of theory on the design of new applications.

## Acknowledgments

LB thanks the financial support from the Spanish Ministerio de Economía y Competitividad (CTQ2015-69363-P). RCO acknowledges the support from the EPSRC (EP/R029385/1) and the Materials Chemistry Consortium (EP/L000202).

## Conflict of interest

The authors declare no conflict of interest.

**Keywords:** aggregation-induced emission · conical intersections · fluorescence · intermolecular interactions · potential energy surfaces

- [1] J. Shi, L. E. Aguilar Suarez, S. J. Yoon, S. Varghese, C. Serpa, S. Y. Park, L. Lüer, D. Roca-Sanjuán, B. Milián-Medina, J. Gierschner, *J. Phys. Chem. C* **2017**, *121*, 23166–23183.
- [2] M. Klessinger, J. Michl, *Excited States and Photochemistry of Organic Molecules*, VCH Publishers, Inc., New York, **1995**.
- [3] J. Luo, Z. Xie, J. W. Y. Lam, L. Cheng, H. Chen, C. Qiu, H. S. Kwok, X. Zhan, Y. Liu, D. Zhu, B. Z. Tang, *Chem. Commun.* **2001**, 1740–1741.
- [4] Z. He, C. Ke, B. Z. Tang, *ACS Omega* **2018**, *3*, 3267–3277.
- [5] J. Mei, N. L. C. Leung, R. T. K. Kwok, J. W. Y. Lam, B. Z. Tang, *Chem. Rev.* **2015**, *115*, 11718–11940.
- [6] J. Mei, Y. Hong, J. W. Y. Lam, A. Qin, Y. Tang, B. Z. Tang, *Adv. Mater.* **2014**, *26*, 5429–5479.
- [7] B. Tang, H. Liu, F. Li, Y. Wang, H. Zhang, *Chem. Commun.* **2016**, *52*, 6577–6580.
- [8] Y. Hong, J. W. Y. Lam, B. Z. Tang, *Chem. Commun.* **2009**, 4332–4353.
- [9] Y. Hong, J. W. Y. Lam, B. Z. Tang, *Chem. Soc. Rev.* **2011**, *40*, 5361–5388.
- [10] Q. Peng, Z. Shuai in *Aggregation-Induced Emission: Materials and Applications* (Ed.: M. Fujiki), American Chemical Society, Washington, DC, **2016**, pp. 35–59.
- [11] Y. Niu, W. Li, Q. Peng, H. Geng, Y. Yi, L. Wang, G. Nan, D. Wang, Z. Shuai, *Mol. Phys.* **2018**, *116*, 1078–1090.
- [12] J. Fan, Y. Zhang, Y. Zhou, L. Lin, C. K. Wang, *J. Phys. Chem. C* **2018**, *122*, 2358–2366.
- [13] Z. Shuai, Q. Peng, *Natl. Sci. Rev.* **2017**, *4*, 224–239.
- [14] J. Chen, C. C. W. Law, J. W. Y. Lam, Y. Dong, S. M. F. Lo, I. D. Williams, D. Zhu, B. Z. Tang, *Chem. Mater.* **2003**, *15*, 1535–1546.
- [15] N. L. C. Leung, N. Xie, W. Yuan, Y. Liu, Q. Wu, Q. Peng, Q. Miao, J. W. Y. Lam, B. Z. Tang, *Chem. Eur. J.* **2014**, *20*, 15349–15353.
- [16] Y. Xie, T. Zhang, Z. Li, Q. Peng, Y. Yi, Z. Shuai, *Chem. Asian J.* **2015**, *10*, 2154–2161.
- [17] X. Zhang, J. K. Sørensen, X. Fu, Y. Zhen, G. Zhao, L. Jiang, H. Dong, J. Liu, Z. Shuai, H. Geng, T. Bjørnholm, W. Hu, *J. Mater. Chem. C* **2014**, *2*, 884–890.
- [18] Y. Niu, Q. Peng, C. Deng, X. Gao, Z. Shuai, *J. Phys. Chem. A* **2010**, *114*, 7817–7831.
- [19] C. Deng, Y. Niu, Q. Peng, A. Qin, Z. Shuai, B. Z. Tang, *J. Chem. Phys.* **2011**, *135*, 014304.
- [20] Z. Shuai, D. Wang, Q. Peng, H. Geng, *Acc. Chem. Res.* **2014**, *47*, 3301–3309.
- [21] Z. Shuai, Q. Peng, *Phys. Rep.* **2014**, *537*, 123–156.
- [22] S. Yin, Q. Peng, Z. Shuai, W. Fang, Y. H. Wang, Y. Luo, *Phys. Rev. B* **2006**, *73*, 1–5.
- [23] Q. Peng, Y. Yi, Z. Shuai, J. Shao, *J. Am. Chem. Soc.* **2007**, *129*, 9333–9339.
- [24] W. Li, L. Zhu, Q. Shi, J. Ren, Q. Peng, Z. Shuai, *Chem. Phys. Lett.* **2017**, *683*, 507–514.
- [25] T. Zhang, Q. Peng, C. Quan, H. Nie, Y. Niu, Y. Xie, Z. Zhao, B. Z. Tang, Z. Shuai, *Chem. Sci.* **2016**, *7*, 5573–5580.
- [26] X. Zheng, Q. Peng, L. Zhu, Y. Xie, X. Huang, Z. Shuai, *Nanoscale* **2016**, *8*, 15173–15180.
- [27] T. Zhang, H. Ma, Y. Niu, W. Li, D. Wang, Q. Peng, Z. Shuai, W. Z. Liang, *J. Phys. Chem. C* **2015**, *119*, 5040–5047.
- [28] G. Yui, S. Yin, Y. Liu, J. Chen, X. Xu, X. Sun, D. Ma, X. Zhan, Q. Peng, Z. Shuai, B. Tang, D. Zhu, W. Fang, Y. Luo, *J. Am. Chem. Soc.* **2005**, *127*, 6335–6346.
- [29] L. Lin, J. Fan, L. Cai, C.-K. Wang, *RSC Adv.* **2017**, *7*, 44089–44096.
- [30] T. Zhang, H. Ma, Y. Niu, W. Li, D. Wang, Q. Peng, Z. Shuai, W. Liang, *J. Phys. Chem. C* **2015**, *119*, 5040–5047 ■ duplicate of ref. 27. ■ ■.
- [31] H. Nie, K. Hu, Y. Cai, Q. Peng, Z. Zhao, R. Hu, J. Chen, S.-J. Su, A. Qin, B. Z. Tang, *Mater. Chem. Front.* **2017**, *1*, 1125–1129.
- [32] Y. C. Duan, Y. Wu, J. L. Jin, D. M. Gu, Y. Geng, M. Zhang, Z. M. Su, *ChemPhysChem* **2017**, *18*, 755–762.
- [33] G. Yu, S. Yin, Y. Liu, J. Chen, X. Xu, X. Sun, D. Ma, X. Zhan, Q. Peng, Z. Shuai, B. Tang, D. Zhu, W. Fang, Y. Luo, *J. Am. Chem. Soc.* **2005**, *127*, 6335–6346 ■ duplicate of ref. 28. ■ ■.
- [34] A. Garzón, A. Navarro, D. López, J. Perles, E. M. García-Frutos, *J. Phys. Chem. C* **2017**, *121*, 27071–27081.
- [35] Y. Niu, Q. Peng, Z. Shuai, *Sci. China Ser. B* **2008**, *51*, 1153–1158.
- [36] T. Zhang, Q. Peng, C. Quan, H. Nie, Y. Niu, Y. Xie, Z. Zhao, B. Z. Tang, Z. Shuai, *Chem. Sci.* **2016**, *7*, 5573–5580 ■ duplicate of ref. 25. ■ ■.

- [37] L. Blancafort, F. Ogliaro, M. Olivucci, M. A. Robb, M. J. Bearpark, A. Sincropi in *Computational Methods in Photochemistry, Vol. 13* (Ed.: A. G. Kutateladze), Taylor & Francis, Boca Raton, FL, **2005**, pp. 31–110.
- [38] X.-L. Peng, S. Ruiz-Barragan, Z.-S. Li, Q.-S. Li, L. Blancafort, *J. Mater. Chem. C* **2016**, *4*, 2802–2810.
- [39] *Conical Intersections: Theory, Computation & Experiment, Advanced Series in Physical Chemistry, Vol. 17* (Eds.: W. Domcke, D. Yarkony, H. Köppel), World Scientific, Singapore, **2011**.
- [40] D. R. Yarkony, *J. Phys. Chem. A* **2001**, *105*, 6277–6293.
- [41] *Conical Intersections: Electronic Structure, Dynamics & Spectroscopy, Advanced Series in Physical Chemistry, Vol. 15* (Eds.: W. Domcke, D. Yarkony, H. Köppel), World Scientific, Singapore, **2004**.
- [42] F. Bernardi, M. Olivucci, M. A. Robb, *Chem. Soc. Rev.* **1996**, *25*, 321–328.
- [43] Q. Li, L. Blancafort, *Chem. Commun.* **2013**, *49*, 5966–5968.
- [44] Y. J. Gao, X. P. Chang, X. Y. Liu, Q. S. Li, G. Cui, W. Thiel, *J. Phys. Chem. A* **2017**, *121*, 2572–2579.
- [45] S. Sasaki, S. Suzuki, W. M. C. Sameera, K. Igawa, K. Morokuma, G. Koinishi, *J. Am. Chem. Soc.* **2016**, *138*, 8194–8206.
- [46] S. Suzuki, S. Maeda, K. Morokuma, *J. Phys. Chem. A* **2015**, *119*, 11479–11487.
- [47] B. Wang, X. Wang, W. Wang, F. Liu, *J. Phys. Chem. C* **2016**, *120*, 21850–21857.
- [48] M. G. S. Londeborough, J. Dolanský, L. Cerdán, K. Lang, T. Jelínek, J. M. Oliva, D. Hnyk, D. Roca-Sanjuán, A. Francés-Monerris, J. Martinčík, M. Nikl, J. D. Kennedy, *Adv. Opt. Mater.* **2017**, *5*, 1600694.
- [49] M. Dommett, M. Rivera, R. Crespo-Otero, *J. Phys. Chem. Lett.* **2017**, *8*, 6148–6153.
- [50] Y. Shigemitsu, T. Mutai, H. Houjou, K. Araki, *J. Phys. Chem. A* **2012**, *116*, 12041–12048.
- [51] R. Crespo-Otero, M. Barbatti, *Chem. Rev.* **2018**, *118*, 7026–7068.
- [52] X. Gao, Q. Peng, Y. Niu, D. Wang, Z. Shuai, *Phys. Chem. Chem. Phys.* **2012**, *14*, 14207–14216.
- [53] A. Prlj, N. Došlić, C. Corminboeuf, *Phys. Chem. Chem. Phys.* **2016**, *18*, 11606–11609.
- [54] H. Lischka, D. Nachtigallová, A. J. A. Aquino, P. G. Szalay, F. Plasser, F. B. C. Machado, M. Barbatti, *Chem. Rev.* **2018**, *118*, 7293–7361.
- [55] M. Barbatti, R. Crespo-Otero in *Density-Functional Methods for Excited States, Topics in Current Chemistry, Vol. 36*, Springer, Cham, **2014**, pp. 415–444.
- [56] A. Dreuw, M. Head-Gordon, *J. Am. Chem. Soc.* **2004**, *126*, 4007–4016.
- [57] Y. Shao, M. Head-Gordon, A. I. Krylov, *J. Chem. Phys.* **2003**, *118*, 4807–4818.
- [58] H. Tong, Y. Dong, Y. Hong, M. Haussier, J. W. Y. Lam, H. H. Y. Sung, X. Yu, J. Sun, I. D. Williams, H. S. Kwok, B. Z. Tang, *J. Phys. Chem. C* **2007**, *111*, 2287–2294.
- [59] L. Blancafort, *ChemPhysChem* **2014**, *15*, 3166–3181.
- [60] F. Sicilia, M. J. Bearpark, L. Blancafort, M. A. Robb, *Theor. Chem. Acc.* **2007**, *118*, 241–251.
- [61] S. Ruiz-Barragan, K. Morokuma, L. Blancafort, *J. Chem. Theory Comput.* **2015**, *11*, 1585–1594.
- [62] E. Cariati, V. Lanzani, E. Tordin, R. Ugo, C. Botta, A. Giacometti Schieroni, A. Sironi, D. Pasini, *Phys. Chem. Chem. Phys.* **2011**, *13*, 18005–18014.
- [63] Y. Dong, J. W. Y. Lam, A. Qin, J. Liu, Z. Li, B. Z. Tang, J. Sun, H. S. Kwok, *Appl. Phys. Lett.* **2007**, *91*, 011111.
- [64] Y. Cai, L. Du, K. Samedov, X. Gu, F. Qi, H. H. Y. Sung, B. O. Patrick, Z. Yan, X. Jiang, H. Zhang, J. W. Y. Lam, I. D. Williams, D. L. Phillips, A. Qin, B. Z. Tang, *Chem. Sci.* **2018**, *9*, 4662–4670.
- [65] B. Xu, J. He, Y. Mu, Q. Zhu, S. Wu, Y. Wang, Y. Zhang, C. Jin, C. Lo, Z. Chi, A. Lien, S. Liu, J. Xu, *Chem. Sci.* **2015**, *6*, 3236–3241.
- [66] K. Kokado, T. Machida, T. Iwasa, T. Taketsugu, K. Sada, *J. Phys. Chem. C* **2018**, *122*, 245–251.
- [67] B. Z. Tang, X. Zhan, G. Yu, P. P. Sze Lee, Y. Liu, D. Zhu, *J. Mater. Chem.* **2001**, *11*, 2974–2978.
- [68] F. Sicilia, L. Blancafort, M. J. Bearpark, M. A. Robb, *J. Phys. Chem. A* **2007**, *111*, 2182–2192.
- [69] Q. Li, D. Mendive-Tapia, M. J. Paterson, A. Migani, M. J. Bearpark, M. A. Robb, L. Blancafort, *Chem. Phys.* **2010**, *377*, 60–65.
- [70] C. Yuan, S. Saito, C. Camacho, S. Irle, I. Hisaki, S. Yamaguchi, *J. Am. Chem. Soc.* **2013**, *135*, 8842–8845.
- [71] C. Yuan, S. Saito, C. Camacho, T. Kowalczyk, S. Irle, S. Yamaguchi, *Chem. Eur. J.* **2014**, *20*, 2193–2200.
- [72] S. Maeda, K. Ohno, K. Morokuma, *Phys. Chem. Chem. Phys.* **2013**, *15*, 3683–3701.
- [73] Y. Harabuchi, S. Maeda, T. Taketsugu, N. Minezawa, K. Morokuma, *J. Chem. Theory Comput.* **2013**, *9*, 4116–4123.
- [74] B. Ventura, Y. M. Poronik, I. Deperasińska, D. T. Gryko, *Chem. Eur. J.* **2016**, *22*, 15380–15388.
- [75] Y. M. Poronik, D. T. Gryko, *Chem. Commun.* **2014**, *50*, 5688–5690.
- [76] A. J. Stasyuk, P. J. Cywiński, D. T. Gryko, *J. Photochem. Photobiol. C* **2016**, *28*, 116–137.
- [77] A. L. Sobolewski, W. Domcke, C. Hättig, *J. Phys. Chem. A* **2006**, *110*, 6301–6306.
- [78] A. L. Sobolewski, W. Domcke, *Phys. Chem. Chem. Phys.* **2006**, *8*, 3410–3417.
- [79] M. Dommett, R. Crespo-Otero, *Phys. Chem. Chem. Phys.* **2017**, *19*, 2409–2416.
- [80] L. Jiang, S. Cao, P. P. H. Cheung, X. Zheng, C. W. T. Leung, Q. Peng, Z. Shuai, B. Z. Tang, S. Yao, X. Huang, *Nat. Commun.* **2017**, *8*, 1.
- [81] X. Cheng, Y. Zhang, S. Han, F. Li, H. Zhang, Y. Wang, *Chem. Eur. J.* **2016**, *22*, 4899–4903.
- [82] Y. Shigemitsu, T. Mutai, H. Houjou, K. Araki, *Phys. Chem. Chem. Phys.* **2014**, *16*, 14388–14395.
- [83] P. Srujana, T. P. Radhakrishnan, *Mater. Chem. Front.* **2018**, *2*, 632–634.
- [84] P. Srujana, T. P. Radhakrishnan, *Chem. Eur. J.* **2018**, *24*, 1784–1788.
- [85] M. Kasha, *Source Radiat. Res. Radiat. Res.* **1963**, *20*, 55–70.
- [86] J. Gierschner, L. Lüer, B. Milián-Medina, D. Oelkrug, H. J. Egelhaaf, *J. Phys. Chem. Lett.* **2013**, *4*, 2686–2697.
- [87] J. Gierschner, S. Varghese, S. Y. Park, *Adv. Opt. Mater.* **2016**, *4*, 348–364.
- [88] N. J. Hestand, F. C. Spano, *Chem. Rev.* **2018**, *118*, 7069–7163.
- [89] J. Gierschner, S. Y. Park, *J. Mater. Chem. C* **2013**, *1*, 5818–5832.
- [90] T. Mutai, H. Shono, Y. Shigemitsu, K. Araki, *CrystEngComm* **2014**, *16*, 3890–3895.
- [91] X. Cheng, K. Wang, S. Huang, H. Zhang, H. Zhang, Y. Wang, *Angew. Chem. Int. Ed.* **2015**, *54*, 8369–8373; *Angew. Chem.* **2015**, *127*, 8489–8493.
- [92] M. Dommett, R. Crespo-Otero, *Phys. Chem. Chem. Phys.* **2017**, *19*, 2409–2416. ■ duplicate of ref. 79. ■ ■.
- [93] H. Ma, W. Shi, J. Ren, W. Li, Q. Peng, Z. Shuai, *J. Phys. Chem. Lett.* **2016**, *7*, 2893–2898.
- [94] D. Presti, L. Wilbraham, C. Targa, F. Labat, A. Pedone, M. C. Menziani, I. Ciofini, C. Adamo, *J. Phys. Chem. C* **2017**, *121*, 5747–5752.
- [95] L. Wilbraham, M. Louis, D. Alberga, A. Brosseau, R. Guillot, F. Ito, F. Labat, R. Métivier, C. Allain, I. Ciofini, *Adv. Mater.* **2018**, *30*, 1800817.
- [96] A. Bernet, R. Q. Albuquerque, M. Behr, S. T. Hoffmann, H. W. Schmidt, *Soft Matter* **2012**, *8*, 66–69.
- [97] H. Zhang, X. Zheng, N. Xie, Z. He, J. Liu, N. L. C. Leung, Y. Niu, X. Huang, K. S. Wong, R. T. K. Kwok, H. H. Y. Sung, I. D. Williams, A. Qin, J. W. Y. Lam, B. Z. Tang, *J. Am. Chem. Soc.* **2017**, *139*, 16264–16272.
- [98] J. Sturala, M. K. Etherington, A. N. Bismillah, H. F. Higginbotham, W. Trewby, J. A. Aguilar, E. H. C. Bromley, A. J. Vestro, A. P. Monkman, P. R. McGonigal, *J. Am. Chem. Soc.* **2017**, *139*, 17882–17889.
- [99] L. Viglianti, N. L. C. Leung, N. Xie, X. Gu, H. H. Y. Sung, Q. Miao, I. D. Williams, E. Licandro, B. Z. Tang, *Chem. Sci.* **2017**, *8*, 2629–2639.
- [100] Y. Gong, Y. Tan, J. Mei, Y. Zhang, W. Yuan, Y. Zhang, J. Sun, B. Z. Tang, *Sci. China Chem.* **2013**, *56*, 1178–1182.
- [101] X. Chen, W. Luo, H. Ma, Q. Peng, W. Z. Yuan, Y. Zhang, *Sci. China Chem.* **2018**, *61*, 351–359.
- [102] R. Ye, Y. Liu, H. Zhang, H. Su, Y. Zhang, L. Xu, R. Hu, R. T. K. Kwok, K. S. Wong, J. W. Y. Lam, W. A. Goddard III, B. Z. Tang, *Polym. Chem.* **2017**, *8*, 1722–1727.
- [103] R. Improta, F. Santoro, L. Blancafort, *Chem. Rev.* **2016**, *116*, 3540–3593.
- [104] K. Saita, M. Takagi, Y. Harabuchi, H. Okada, S. Maeda, *J. Chem. Phys.* **2018**, *149*, 072329.

Manuscript received: November 8, 2018

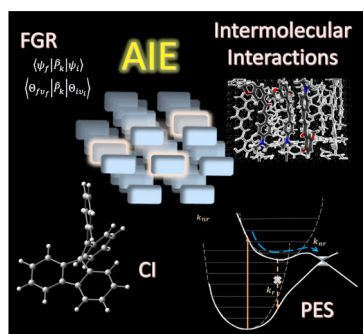
Revised manuscript received: December 7, 2018

Accepted manuscript online: December 10, 2018

Version of record online: ■ ■ ■ 0000


## MINIREVIEW

**Emission in aggregate:** Theory has been important to understand aggregation-induced emission. This review focuses on potential energy surface studies and the restricted access to a conical intersection model. It discusses the complementarities with the restriction of intramolecular motion model and Fermi golden rule based calculations. The role of intermolecular interactions is also highlighted.



Rachel Crespo-Otero,\* Quansong Li,  
Lluís Blancafort\*

■ ■ - ■ ■ ■  
**Exploring Potential Energy Surfaces  
for Aggregation-Induced Emission—  
From Solution to Crystal**

 Review focusing on potential energy surfaces and the restricted access to conical intersection model to understand aggregation-induced emission **SPACE RESERVED FOR IMAGE AND LINK**

Share your work on social media! *Chemistry – An Asian Journal* has added Twitter as a means to promote your article. Twitter is an online microblogging service that enables its users to send and read short messages and media, known as tweets. Please check the pre-written tweet in the galley proofs for accuracy. If you, your team, or institution have a Twitter account, please include its handle @username. Please use hashtags only for the most important keywords, such as #catalysis, #nanoparticles, or #proteindesign. The ToC picture and a link to your article will be added automatically, so the **tweet text must not exceed 250 characters**. This tweet will be posted on the journal's Twitter account (follow us @ChemAsianJ) upon publication of your article in its final (possibly unpaginated) form. We recommend you to retweet it to alert more researchers about your publication, or to point it out to your institution's social media team.

Please check that the ORCID identifiers listed below are correct. We encourage all authors to provide an ORCID identifier for each coauthor. ORCID is a registry that provides researchers with a unique digital identifier. Some funding agencies recommend or even require the inclusion of ORCID IDs in all published articles, and authors should consult their funding agency guidelines for details. Registration is easy and free; for further information, see <http://orcid.org/>.

Dr. Rachel Crespo-Otero <http://orcid.org/0000-0002-8725-5350>

Prof. Quansong Li <http://orcid.org/0000-0002-1462-5410>

Prof. Lluís Blancafort <http://orcid.org/0000-0002-0003-5540>